

Supporting Information

for

Interfacial engineering of polymer - MOF composite by *in situ* vitrification

Rijia Lin,^a Jingwei Hou,^{*a} Mengran Li,^a Zhanke Wang,^a Lei Ge,^b Shichun Li,^c Simon Smart,^{a,d} Zhonghua Zhu,^a Thomas D. Bennett,^e Vicki Chen^a

^a School of Chemical Engineering, The University of Queensland, Brisbane 4072 Australia

^b Centre for Future Materials, University of Southern Queensland, Queensland 4300, Australia

^c Institute of Chemical Materials, China Academy of Engineering Physics, Mianyang 621900, PR China

^d Dow Centre for Sustainable Engineering Innovation, The University of Queensland, QLD 4072, Australia

^e Department of Materials Science and Metallurgy, University of Cambridge, Cambridge, CB3 0FS, UK

Experimental Section

Materials

Zinc nitrate hexahydrate ($\text{Zn}(\text{NO}_3)_2 \cdot 6\text{H}_2\text{O}$), benzimidazole (bIm), and imidazole (Im) were obtained from Sigma-Aldrich. The polyimide 6FDA-DAM ($M_w \sim 270000$, $\text{PDI} \sim 2.68$) was supplied by Akron Polymer Systems. *N,N*-dimethylformamide (DMF), methanol and chloroform were purchased from Merck. All the chemicals were used without further purification. Carbon dioxide, nitrogen gas, and argon were supplied by Coregas.

Synthesis of ZIF-62-bIm_{0.05}

We synthesized non-stoichiometric ZIF-62 $\text{Zn}(\text{Im})_{1.95}(\text{bIm})_{0.05}$ (referred to as ZIF-62-bIm_{0.05}) following the same route as reported elsewhere.¹ In brief, zinc nitrate hexahydrate (1.2 g), imidazole (0.891g) and benzimidazole (0.016g) were dissolved in 90 mL of DMF and transferred into a 100 mL screw-top jar. Subsequently, the jar was heated at 130 °C for 7 d and cooled to room temperature. The obtained crystals were filtered and washed with DMF three times and with methanol three times before being dried in a vacuum oven at 150 °C for 24 h. The as-synthesized ZIF-62- bIm_{0.05} was milled using a ball mill (Fritsch, Pulverisette, Germany) for 1 h at a rotational speed of 800 rpm.

For the melting of pure crystalline ZIF-62-bIm_{0.05}, the sample was placed in a quartz crucible, then heated in a tube furnace with a ramping rate of 20 °C min⁻¹ under Ar protection. Once the temperature reached 390 °C, the sample was cooled back to room temperature under the protection of Ar gas. The sample was referred to as a_gZIF-62-bIm_{0.05} in consistence to our early publications.²

Fabrication of composite

The 6FDA-DAM chloroform solution was prepared by dissolved 0.45 g 6FDA-DAM into 3.5 mL chloroform. Bubbles were removed by ultrasonication for another 10 min. Subsequently, the solution was poured on a flat glass plate, and was cast using a doctor blade with the thickness of 550 μm. The membrane was dried slowly at ambient temperature for 24 h and at 150 °C under vacuum for 24 h.

The composite mixed matrix membranes (MMMs) were prepared following a similar procedure. The suspension was prepared by dispersing a certain amount of ZIF-62-bIm_{0.05} into 3.5 mL chloroform via 15 min sonication, followed by slowly adding 6FDA-DAM (0.45 g) into the suspension under sonication for several times. Subsequently, the suspension was stirred for another 12 h for full dissolution prior to the casting step.

The loading of ZIF-62-bIm_{0.05} in MMMs was adjusted to 10, 20 and 30 wt% based on the equation provided below and named as (ZIF-62)_{0.1}(6FDA-DAM)_{0.9}, (ZIF-62)_{0.2}(6FDA-DAM)_{0.8} and (ZIF-62)_{0.3}(6FDA-DAM)_{0.7}, respectively.

$$\phi = \frac{m_{\text{filler}}}{m_{\text{filler}} + m_{\text{6FDA-DAM}}}$$

where ϕ is the filler loading (%), m_{filler} and $m_{6\text{FDA-DAM}}$ represent the mass of ZIF-62 and mass of polymer in the MMMs, respectively.

For the *in situ* melting, the prepared MMMs with crystal ZIF-62-bIm_{0.05} fillers were heated at a ramping rate of 20 °C min⁻¹ to 390 °C, hold for 5 min, and then cooled back to room temperature under Ar protection. The (ZIF-62)_{0.1}(6FDA-DAM)_{0.9}, (ZIF-62)_{0.2}(6FDA-DAM)_{0.8} and (ZIF-62)_{0.3}(6FDA-DAM)_{0.7} after thermal treatment are referred to as (a_gZIF-62)_{0.1}(6FDA-DAM)_{0.9}, (a_gZIF-62)_{0.2}(6FDA-DAM)_{0.8} and (a_gZIF-62)_{0.3}(6FDA-DAM)_{0.7}, respectively. The pure 6FDA-DAM membrane was also subjected to the same thermal treatment as a benchmark, the 6FDA-DAM membrane after thermal treatment is referred to as t-6FDA-DAM.

The thickness of the neat membrane and MMMs, measured using a micrometre, are within the range of 45–65 μm. Prior to the gas permeation tests and characterizations, the membranes were kept free from moisture with a desiccant.

Characterization

X-ray diffraction (XRD) patterns were collected with a Bruker D8 Advanced X-Ray diffractometer (40 kV, 30 mA) using a Cu K α (λ = 0.15406 nm) radiation source with a 2 theta range between 5° and 40°.

Nuclear magnetic resonance spectroscopy (NMR). The molar ratio of bIm/Im linker in ZIF-62-bIm_x was determined by liquid-state nuclear magnetic resonance spectroscopy (NMR). 6.0 mg of sample was digested in a mixture of DCl/D₂O (35%; 0.1 mL) and DMSO-d₆ (0.5 mL). The ¹H NMR measurement was performed with a Bruker Avance 500 high-resolution NMR spectrometer interfaced to a 11.7 Tesla 51 mm bore magnet system. Chemical shifts were referenced to the residual protiosolvent signals of DMSO-d₆.

Thermogravimetric analysis (TGA) and differential scanning calorimetry (DSC) analysis were conducted using a METTLER TOLEDO TGA/DSC 1 STAR^e System. To determine the melting and decomposition temperature, the sample was heated at a rate of 20 °C min⁻¹ under an Ar atmosphere. To determine the glass transition temperature, in the first up-scan the sample was heated to 450 °C at 20 °C min⁻¹ under an Ar atmosphere. Subsequently, the sample was cooled back to 100 °C at the rate of 10 °C min⁻¹, followed by another heating at a ramp rate of 10 °C min⁻¹. The glass transition temperature (T_g) of the ZIF and polymer was obtained from the second upscan.

X-ray photoelectron spectrometer (XPS) was applied to study the surface chemistry and compositions by Kratos Axis Ultra XPS equipped with a 165mm hemispherical electron energy analyser and a monochromatic Al K α (1486.6eV) radiation at 150W (15kV, 10mA). The C 1s peak position was set to 284.8 eV and taken as an internal standard.

We tested the CO₂ and N₂ adsorption isotherms at 273K and 303K using a Micromeritics TriStar II 3020. Before the test, the samples were degassed at 150 °C for 24 h and then 200 °C for 2 h. The samples were regenerated at 200 °C under 10 mTorr until no further pressure decreased after each run of the measurement. Surface areas and pore size distributions were calculated using the nonlocal density functional theory (NLDFT) model provided in the TriStar

II 3020 software (CO₂, 273 K, carbon with slit-pore geometry).^{1, 3} The isosteric heat of CO₂ adsorption and the ideal adsorbed solution theory (IAST) selectivity were calculated following the procedures mentioned in below.^{4, 5}

A JEOL JSM7100 scanning electron microscope (SEM) was used to characterize the sample morphology at an accelerating voltage of 8 kV. Focused ion beam scanning electron microscopy (FIB-SEM) was performed using an FEI SCIOS FIB/SEM dual beam system to examine the contact of continuous phase with dispersed phase. Details of the method were reported in our previous studies⁶⁻⁹ and can be found below.

Permeation test

The permeability test of the membranes was carried out in a constant-volume permeation system with variable feed pressure, which has also been described in our previous study¹⁰. The membrane was stabilized under vacuum for 5 min prior to the permeation test. When switching the feeding gas, we degassed the membrane for about 15 min to desorb the prior permeate gas. The permeation test was performed with a driving force at 2 bar in the upper stream and at 0.015 bar in the downstream at 30 °C.

The permeation coefficient (P in Barrer) is estimated according to the following equation:

$$P = \frac{273.15 \times 10^{10}}{760AT} \frac{VL}{P_0 \times 76} \frac{dp}{dt} \frac{1}{14.7}$$

where A is permeation area of the membrane (cm²), T denotes the operational temperature (K), V represents the dead volume of the permeation side (cm³), L is the membrane thickness (cm), P₀ is the feeding pressure (psi), and dp/dt stands for the steady rate of pressure rise in the permeation side (mm Hg s⁻¹). 1 Barrer = 1 × 10⁻¹⁰ cm³ (STP) cm cm⁻² s⁻¹ cm Hg⁻¹

The ideal selectivity for one gas pair was estimated following the equation below:

$$\alpha = \frac{P_A}{P_B}$$

where P_A is permeation coefficients of pure gas A, and P_B is permeation coefficients pure gas B.

Isosteric heat of CO₂ adsorption

Adsorption Heat of CO₂ was calculated by the following virial equations.

$$\ln P = \ln q + \frac{1}{T} * \sum_{i=0}^m a_i Q^i$$

$$Q_{st} = -R * \sum_{i=0}^m a_i q^i$$

The above virial expression was used to fit the combined isotherm data for ZIF-62-bIm_{0.05} and a_gZIF-62-bIm_{0.05} at 273K and 298 K, where P is the pressure, q is the adsorbed amount, T is the adsorption temperature, a_i and b_i are virial coefficients, and m and n are the number of coefficients used to describe the isotherms. Q_{st} is the coverage-dependent enthalpy of adsorption and R is the universal gas constant.

CO₂/N₂ selectivity prediction via IAST (Ideal adsorbed solution theory)

The experimental adsorption data for pure CO₂ and N₂ (measured at 303K) were fitted using a Langmuir-Freundlich (L-F) model:

$$q_i = \frac{a \times b \times p_i^{1/n}}{1 + b \times p_i^{1/n}}$$

Where q_i and p_i are adsorbed amounts and pressure of component i , respectively.

The adsorption selectivities for binary mixtures of CO₂/N₂ were calculated using the ideal adsorption solution theory (IAST), which was reported by Myers and Prausnitz (*AIChE J.* 1965, 11, 121.). And the selectivity was defined by:

$$S_{i/j} = \frac{x_i \times y_j}{x_j \times y_i}$$

where x_i is the mole fraction of component i in the adsorbed phase and y_i is the mole fraction of component i in the bulk.

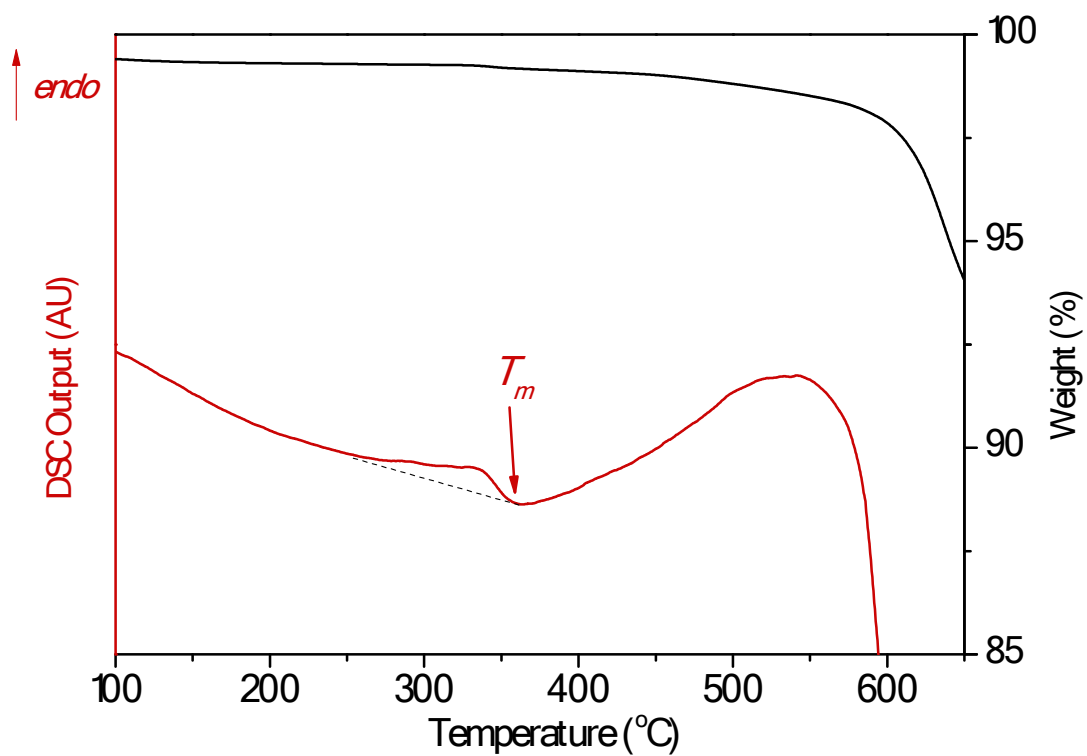


Fig. S1 Thermogravimetric (TG, black) and differential scanning calorimetry (DSC, red) analysis for ZIF-62-bIm_{0.05}

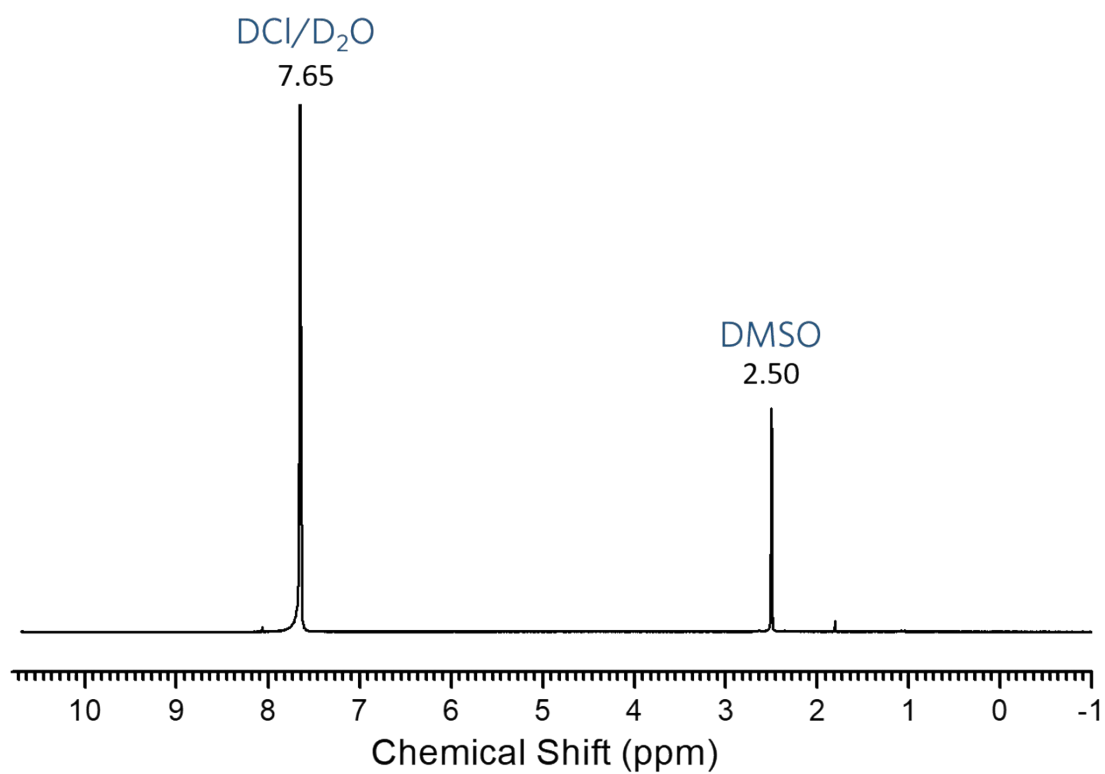


Fig. S2 ^1H NMR spectrum of the DMSO- d_6 solvent (0.5 mL) with DCI/D₂O (35%; 0.1 mL). 7.65 (DCI/D₂O), 2.50 (DMSO)

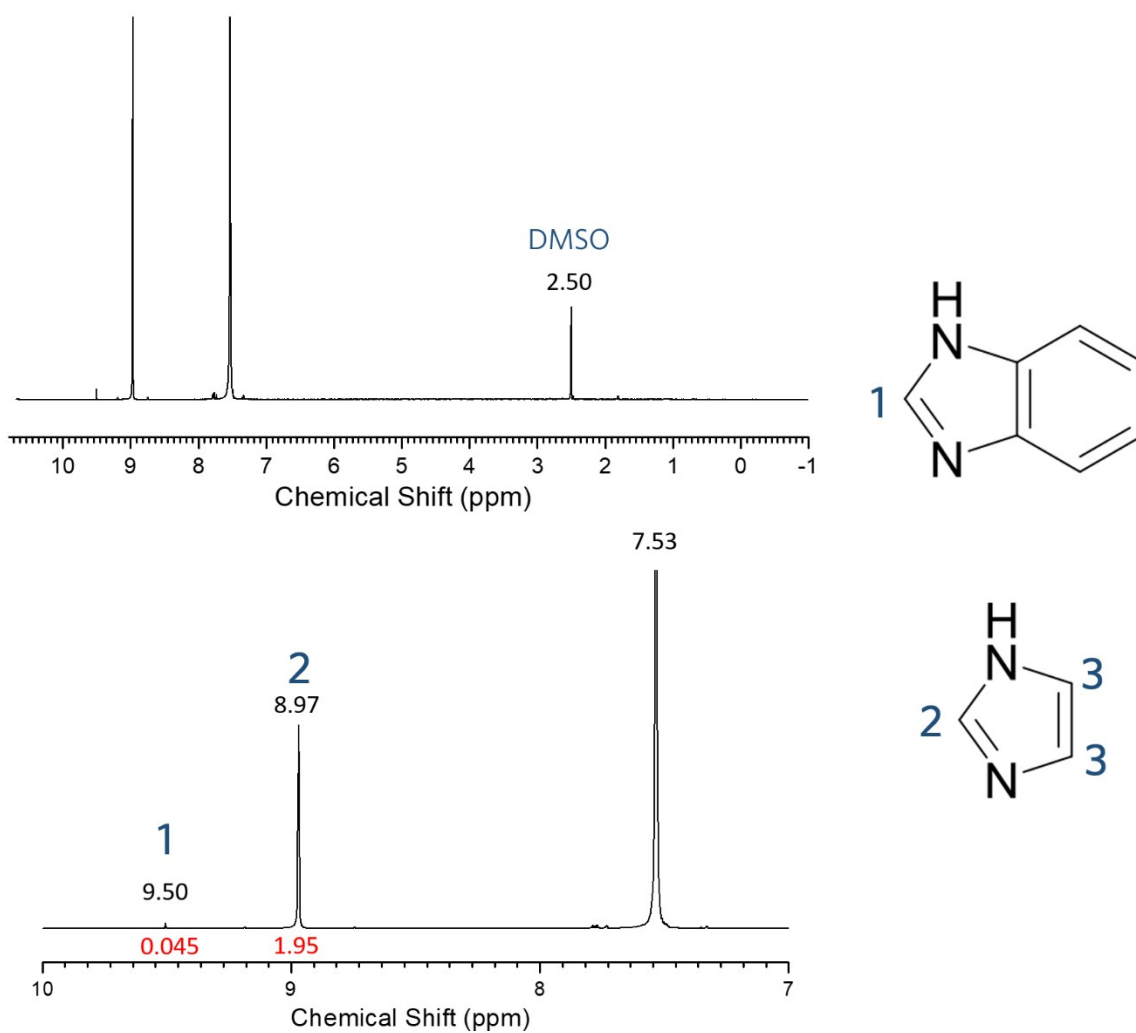


Fig. S3 ^1H NMR spectrum of ZIF-62-bIm_{0.05} digested in DCI/DMSO-d₆. Top figure is the full spectrum and the bottom is a partially enlarged region. Peaks are assigned in the enlarged figure (peak at 7.53 ppm is assigned to the overlap of 3H and DCI/D₂O).

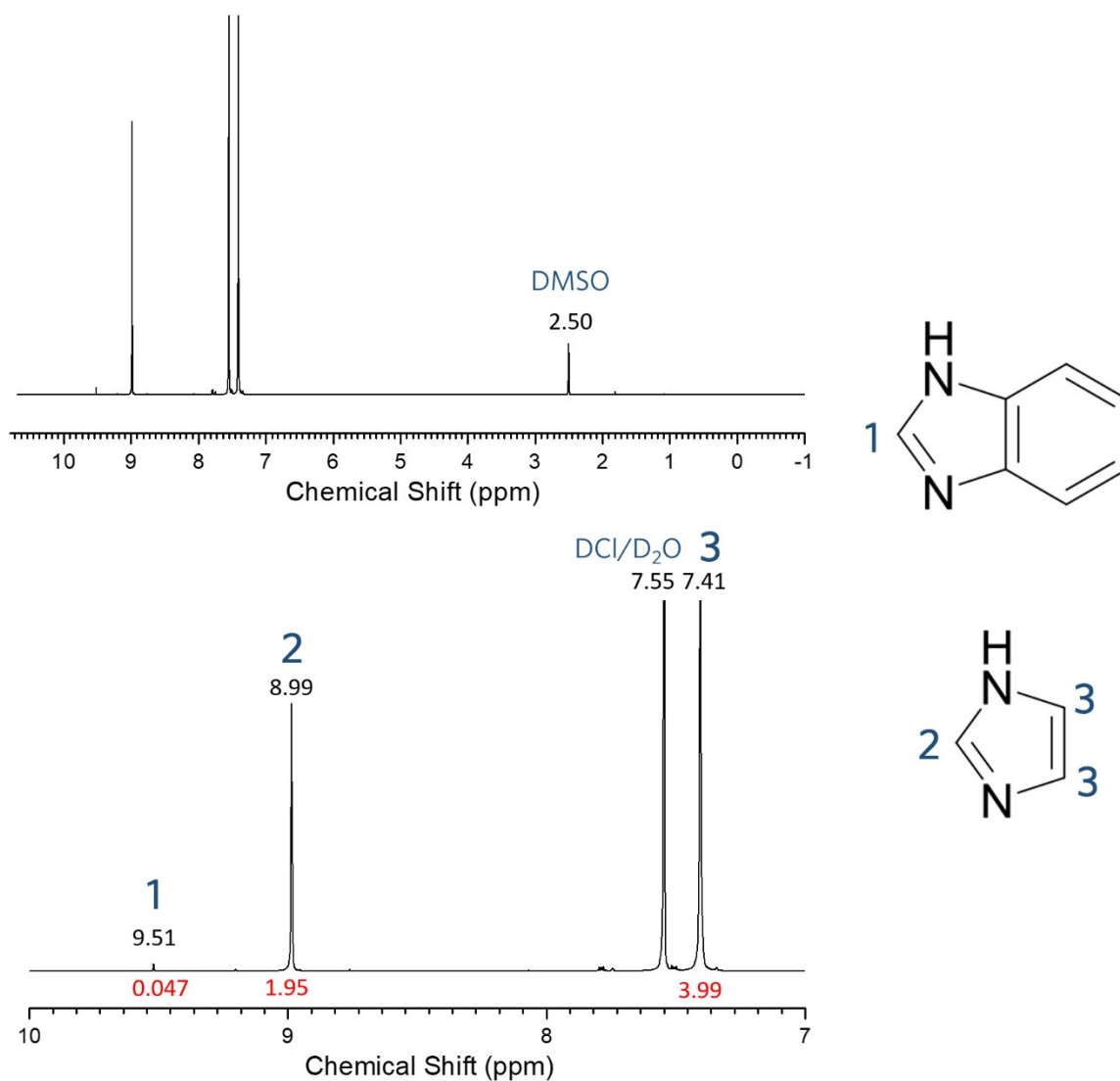


Fig. S4 ^1H NMR spectrum of $a_9\text{ZIF-62-bIm}_{0.05}$ digested in DCI/DMSO- d_6 . Top figure is the full spectrum and the bottom is a partially enlarged region.

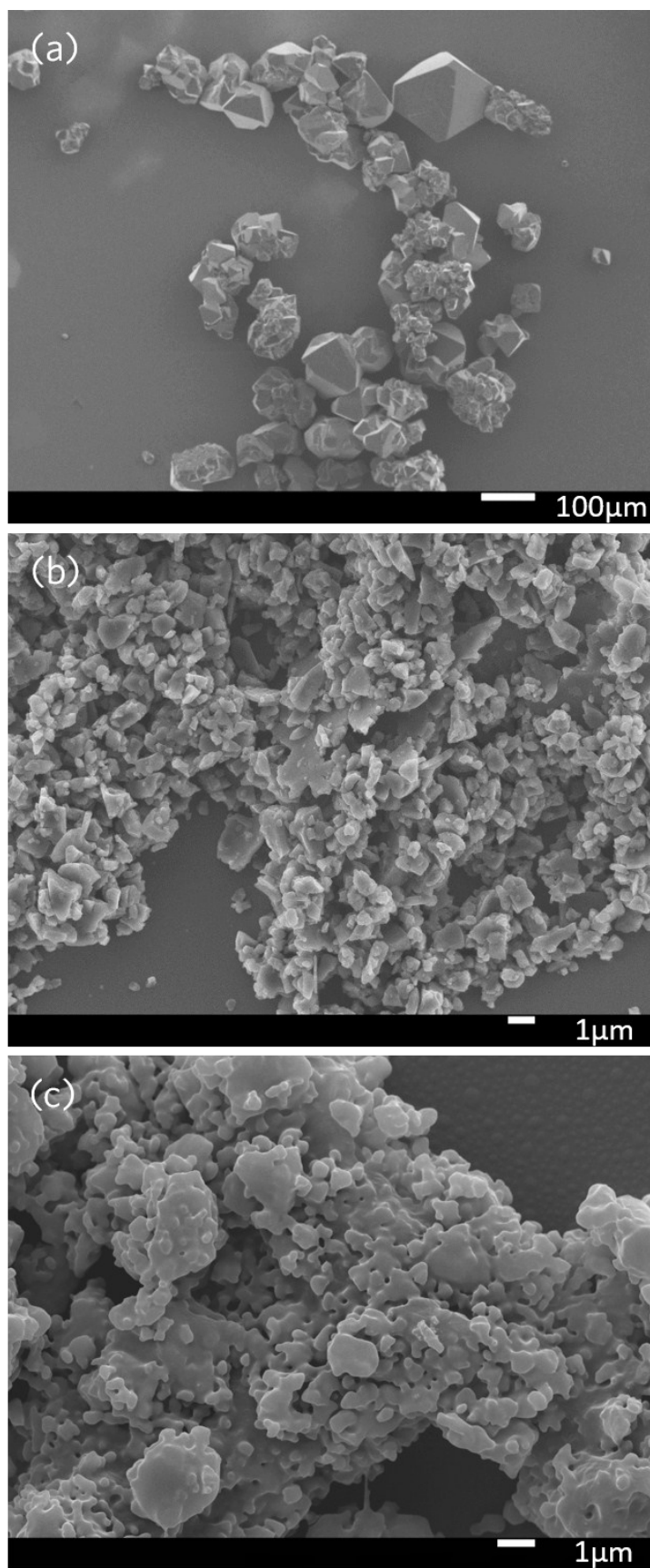


Fig. S5 SEM images of (a) ZIF-62-bIm_{0.05} crystal, (b) ZIF-62-bIm_{0.05} after ball mill treatment, and (c) a_gZIF-62-bIm_{0.05} from melting of the ball-milled crystals

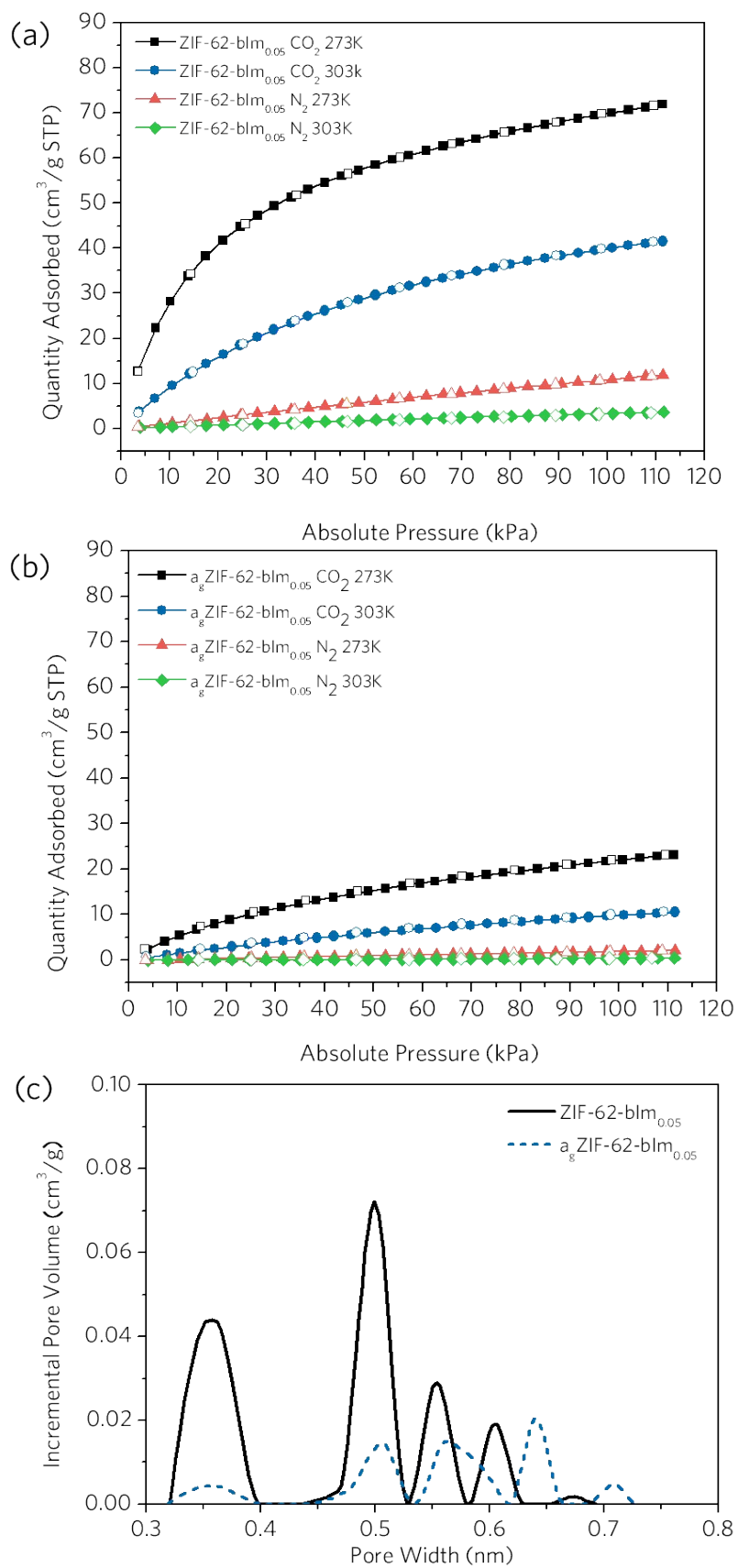


Fig. S6 (a, b) CO₂ and N₂ adsorption isotherms of ZIF-62-bIm_{0.05} crystal (a) and a₈ZIF-62-bIm_{0.05} (b) at 273K and 303 K. Adsorption and desorption are shown as closed and open

symbols, respectively. (c) Pore size distribution of ZIF-62-bIm_{0.05} crystal and a_gZIF-62-bIm_{0.05}

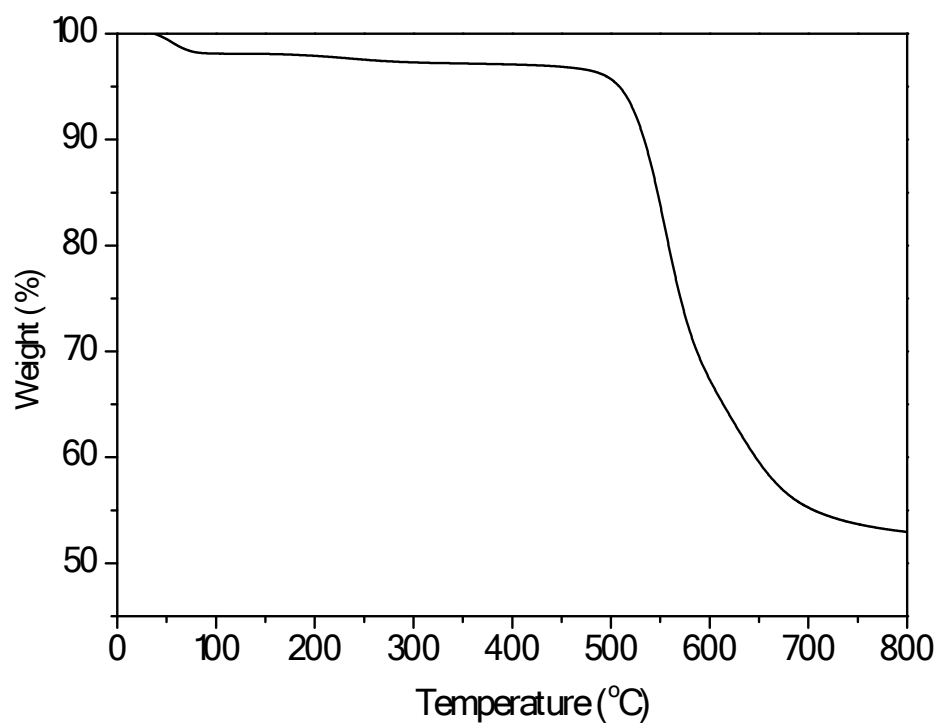


Fig. S7 Thermogravimetric analysis (TGA) for pure 6FDA-DAM.

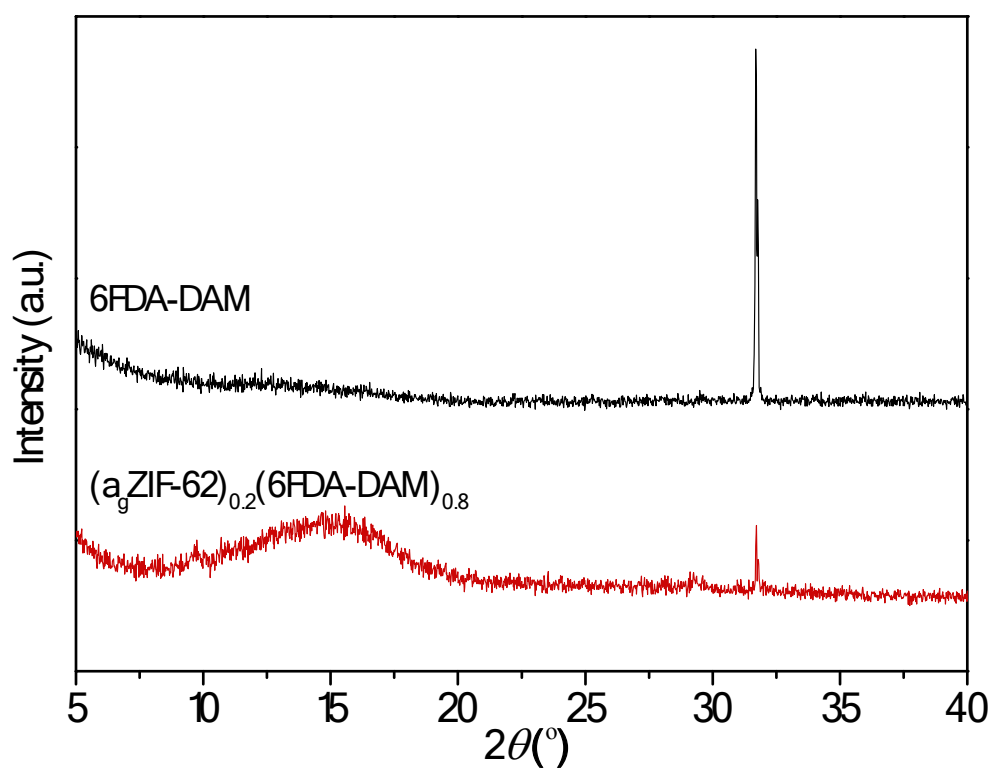


Fig. S8 XRD for pure 6FDA-DAM and nanocomposite membrane (a₉ZIF-62)_{0.2}(6FDA-DAM)_{0.8}.

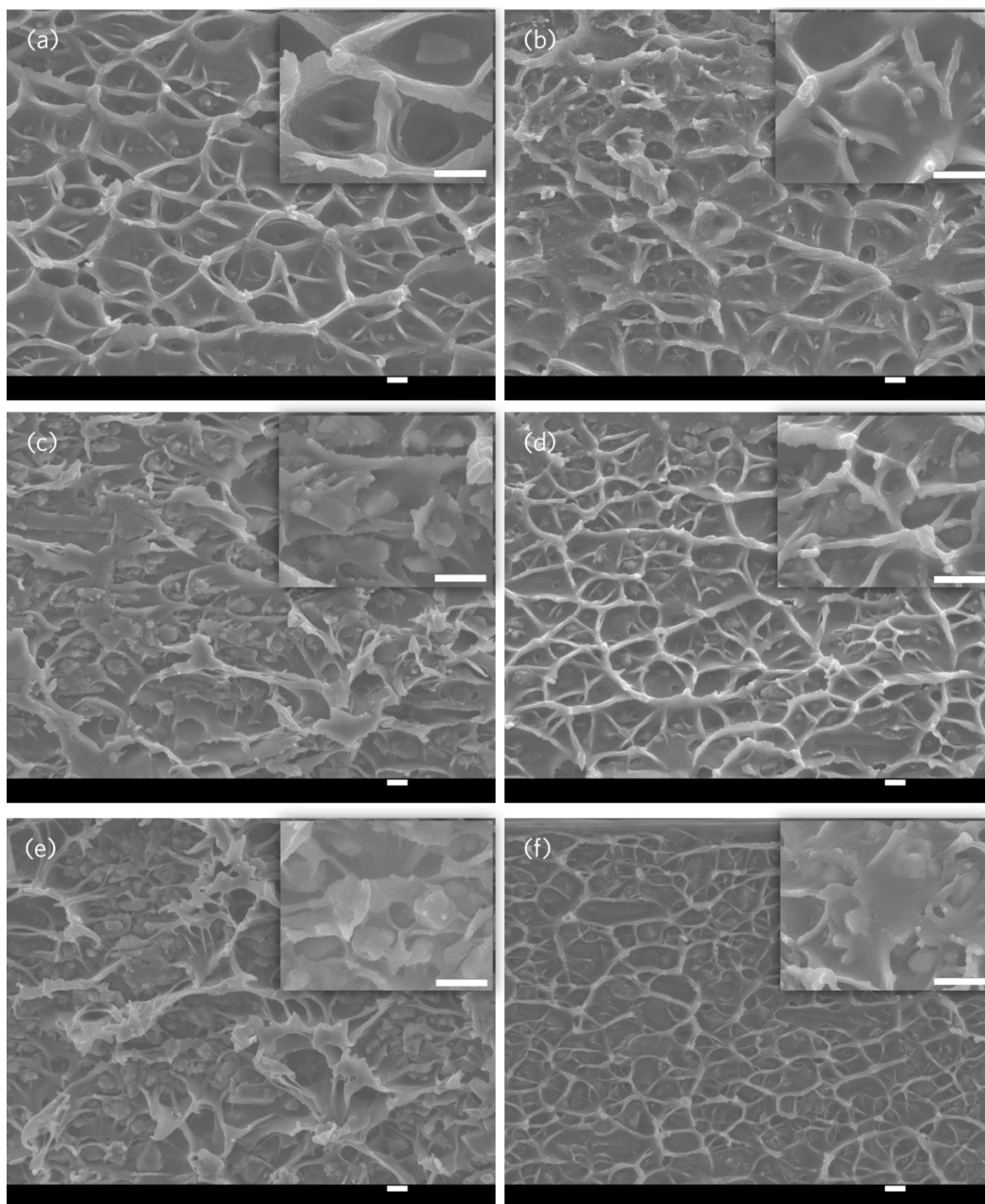


Fig. S9 SEM images of MMM cross-sections with magnified images inserted on top right: (a) $(\text{ZIF-62})_{0.1}(\text{6FDA-DAM})_{0.9}$, (b) $(\text{a}_g\text{ZIF-62})_{0.1}(\text{6FDA-DAM})_{0.9}$, (c) $(\text{ZIF-62})_{0.2}(\text{6FDA-DAM})_{0.8}$, (d) $(\text{a}_g\text{ZIF-62})_{0.2}(\text{6FDA-DAM})_{0.8}$, (e) $(\text{ZIF-62})_{0.3}(\text{6FDA-DAM})_{0.7}$, (f) $(\text{a}_g\text{ZIF-62})_{0.3}(\text{6FDA-DAM})_{0.7}$. All the scale bars are 1 μm .

Details of the FIB-SEM method

The specimen was sputtered with a conducting layer of Pt for 100 s. A trench was milled on the surface of the membrane by using a Ga⁺ focused ion beam (Fig. S7). Serial milling of slices with a thickness of 80 nm were removed from the sample up to a depth of 18 μm by the Ga⁺ FIB at 30 kV and 0.5 nA. A series of exposed cross-section SEM images in back-scattered electron (BSE) imaging mode were collected sequentially during the automatic slice-and-view experiments using an in-lens backscattered electron detector at 2kV. The components of the MMM can be distinguished from the different grayscale in the BSE SEM image. Fillers are brightest whereas polymer appear a medium grayscale, and voids are darker than the polymer matrix. The stack of the images was aligned and reconstructed in three-dimensional to analyse the volume of each phases. A software Avizo (FEI Visualization Sciences Group) was used to reconstruct the images, segment all the phases and calculate the fraction of the 3D volume of each phases. Sizes and spatial resolutions of MMMs in FIB-SEM are shown in Table S1.

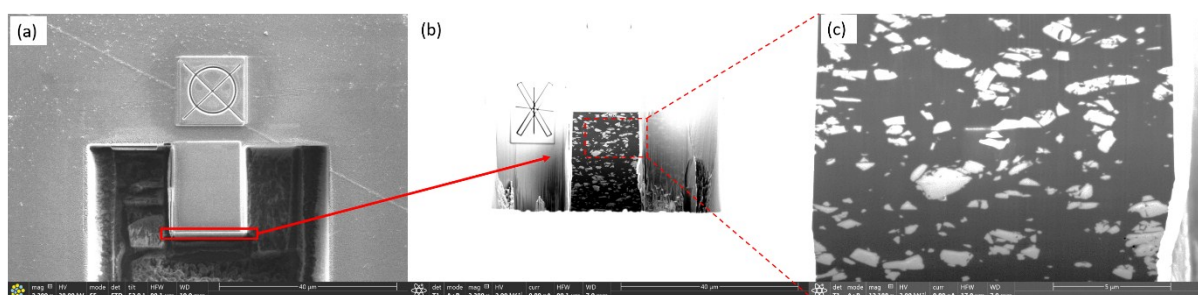


Fig. S10 Typical FIB-SEM images of (ZIF-62)_{0.2}(6FDA-DAM)_{0.8} (a) FIB milling hole (top view), (b) cross-sectional image in the BSE mode (c) magnified image with contrast difference of polymer matrix, filler and interfacial voids.

Table S1 Sizes and spatial resolutions of (ZIF-62)_{0.2}(6FDA-DAM)_{0.8} and (a_gZIF-62)_{0.2}(6FDA-DAM)_{0.8} in FIB-SEM

	X	y	z
(ZIF-62)_{0.2}(6FDA-DAM)_{0.8}			
Sample dimension (μm)	15.6	9.3	15.5
Number of voxels	1494	706	516
(a_gZIF-62)_{0.2}(6FDA-DAM)_{0.8}			
Sample dimension (μm)	14.3	9.2	15.5
Number of voxels	1831	940	516

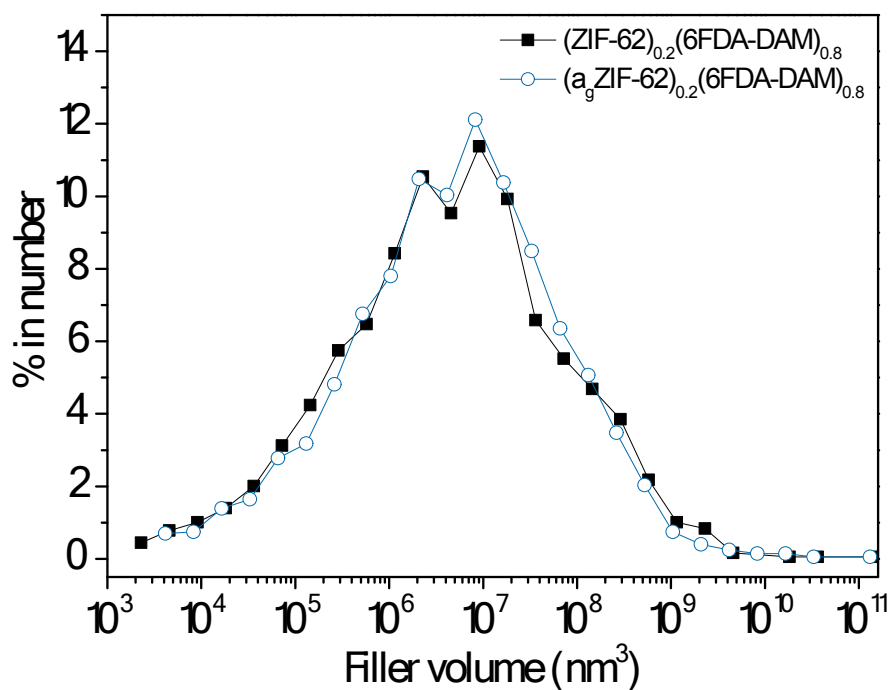


Fig. S11 Filler particle size distribution in $(\text{ZIF-62})_{0.2}(\text{6FDA-DAM})_{0.8}$ and $(\text{a}_9\text{ZIF-62})_{0.2}(\text{6FDA-DAM})_{0.8}$ derived from the image analysis of the FIB-SEM tomogram

Table S2 Volume fraction of different phase in $(\text{ZIF-62})_{0.2}(\text{6FDA-DAM})_{0.8}$ and $(\text{a}_9\text{ZIF-62})_{0.2}(\text{6FDA-DAM})_{0.8}$ derived from the image analysis of the reconstructed FIB-SEM tomogram

	Filler	Polymer	Voids
$(\text{ZIF-62})_{0.2}(\text{6FDA-DAM})_{0.8}$	23.01%	76.97%	0.0204%
$(\text{a}_9\text{ZIF-62})_{0.2}(\text{6FDA-DAM})_{0.8}$	23.09%	76.91%	0.0043%

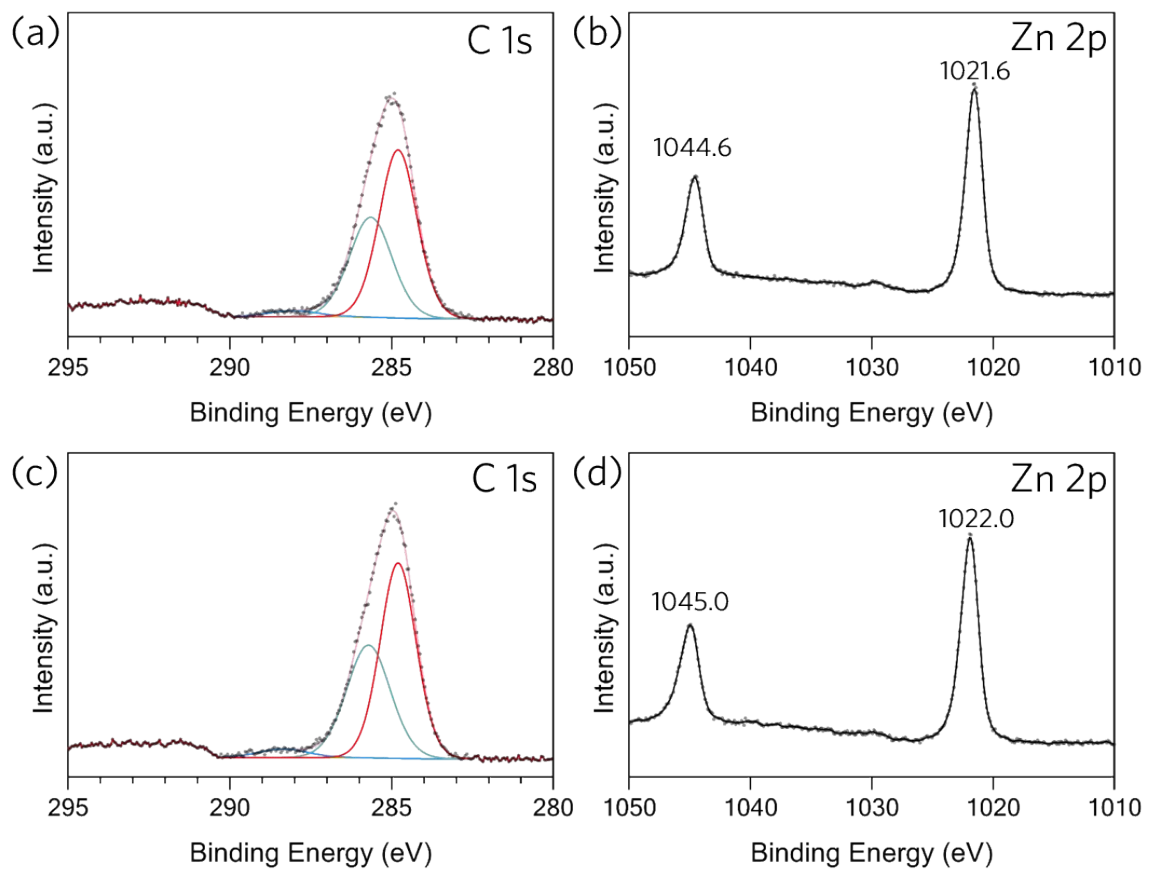


Fig. S12 XPS spectra for ZIF-62-bIm_{0.05} crystal (a: C 1s, b: Zn sp) and ZIF-62-bIm_{0.05} (c: C 1s, d: Zn 2p)

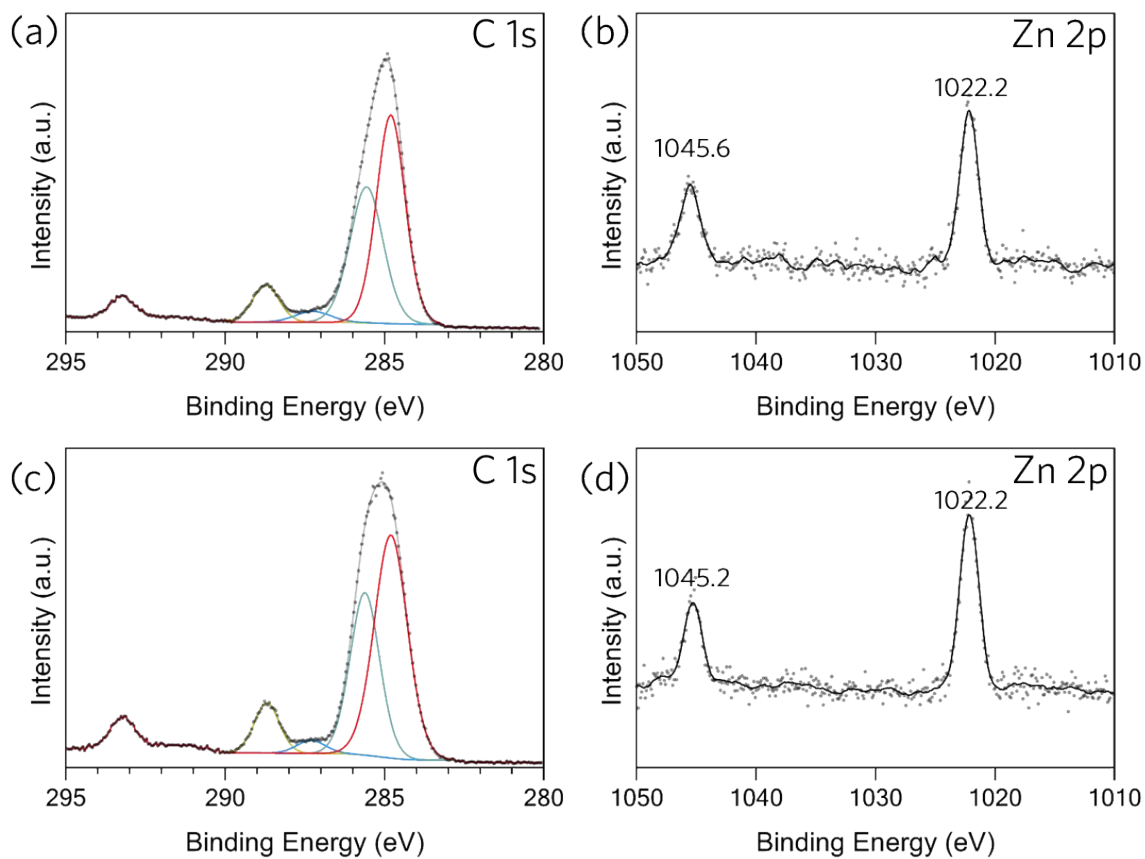


Fig. S13 XPS spectra for $(\text{ZIF-62})_{0.2}(\text{6FDA-DAM})_{0.8}$ (a: C 1s, b: Zn sp) and $(\text{a}_g\text{ZIF-62})_{0.2}(\text{6FDA-DAM})_{0.8}$ (c: C 1s, b: Zn 2p).

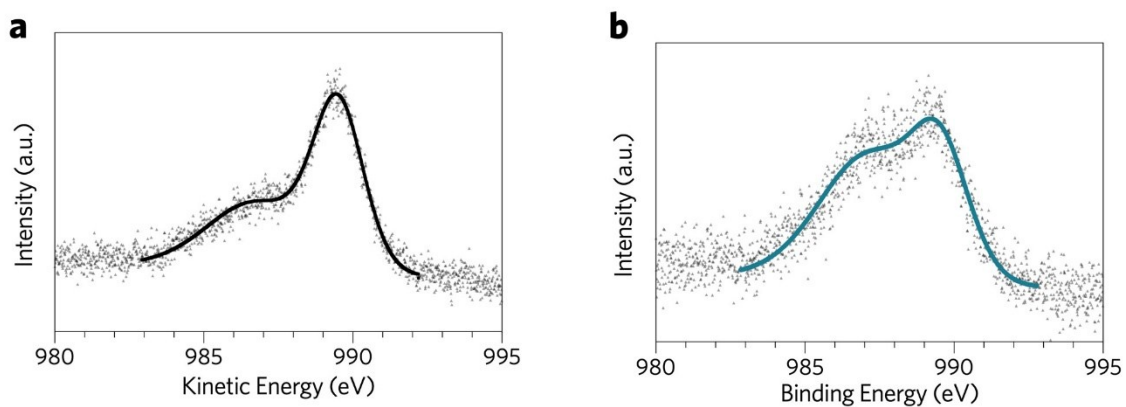


Fig. S14 Zn LMM Auger spectra of (a) $(\text{ZIF-62})_{0.2}(\text{6FDA-DAM})_{0.8}$ and (b) $(\text{a}_g\text{ZIF-62})_{0.2}(\text{6FDA-DAM})_{0.8}$

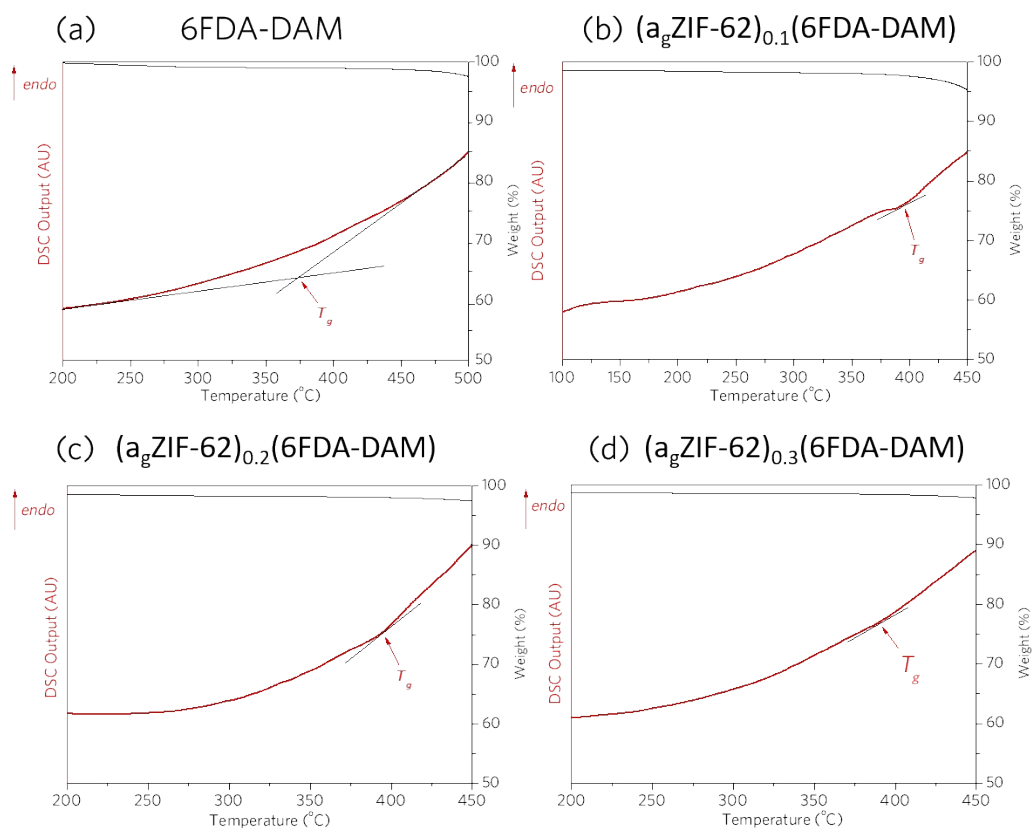


Fig. S15 Thermogravimetric (TG, black) and differential scanning calorimetry (DSC, red) analysis for membrane samples. (a) 6FDA-DAM, (b) $(a_g\text{ZIF-62})_{0.1}(6\text{FDA-DAM})_{0.9}$, (c) $(a_g\text{ZIF-62})_{0.2}(6\text{FDA-DAM})_{0.8}$, (d) $(a_g\text{ZIF-62})_{0.3}(6\text{FDA-DAM})_{0.7}$

Table S3 Glass transition temperature (T_g) of membrane samples obtained from DSC analysis

Sample	T_g (°C)
6FDA-DAM	375.4
$(a_g\text{ZIF-62})_{0.1}(6\text{FDA-DAM})_{0.9}$	387.4
$(a_g\text{ZIF-62})_{0.2}(6\text{FDA-DAM})_{0.8}$	393.3
$(a_g\text{ZIF-62})_{0.3}(6\text{FDA-DAM})_{0.7}$	388.8

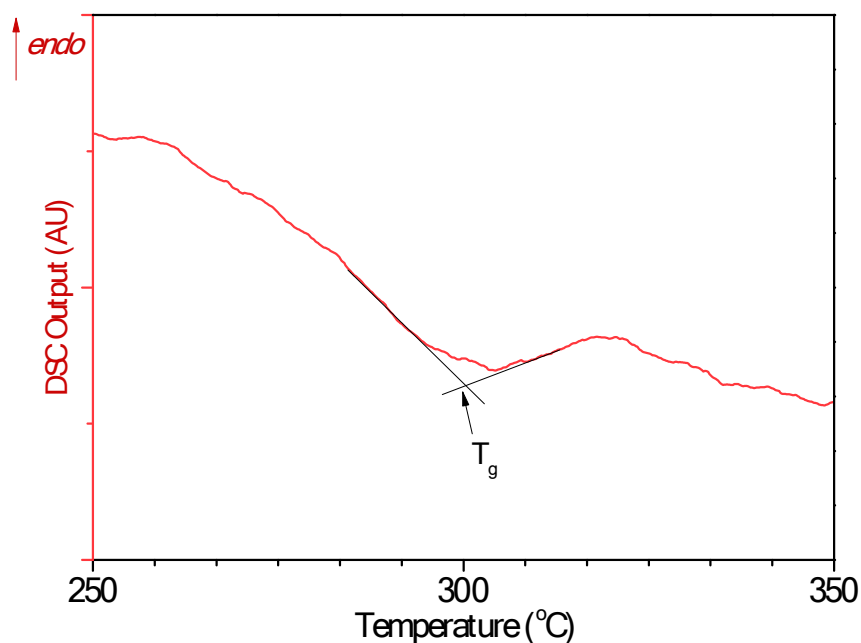


Fig. S16 Differential scanning calorimetry analysis for $a_g\text{ZIF-62-bIm}_{0.05}$.

Table S4 Gas permeability and selectivity of pure 6FDA-DAM membrane, ZIF-62 MMMs and MMMs after thermal treatment

Sample	Permeability (barrer)		Selectivity
	CO ₂	N ₂	CO ₂ /N ₂
6FDA-DAM	752.0±30.1	43.6±3.1	17.2
(ZIF-62) _{0.1} (6FDA-DAM) _{0.9}	609.3±30.7	31.6±1.1	19.3
(ZIF-62) _{0.2} (6FDA-DAM) _{0.8}	678.7±12.3	31.9±3.8	21.3
(ZIF-62) _{0.3} (6FDA-DAM) _{0.7}	755.0±20.5	42.7±1.8	17.7
t-6FDA-DAM	741.5±30.1	41.4±1.8	17.9
($a_g\text{ZIF-62}$) _{0.1} (6FDA-DAM) _{0.9}	579.8±14.9	26.5±1.8	21.9
($a_g\text{ZIF-62}$) _{0.2} (6FDA-DAM) _{0.8}	587.3±43.0	21.7±2.2	27.1
($a_g\text{ZIF-62}$) _{0.3} (6FDA-DAM) _{0.7}	461.2±36.2	19.5±2.3	23.7

References

1. L. Frentzel-Beyme, M. Kloss, P. Kolodzeiski, R. Pallach and S. Henke, *J. Am. Chem. Soc.*, 2019, **141**, 12362-12371.
2. T. D. Bennett, Y. Yue, P. Li, A. Qiao, H. Tao, N. G. Greaves, T. Richards, G. I. Lampronti, S. A. Redfern, F. Blanc, O. K. Farha, J. T. Hupp, A. K. Cheetham and D. A. Keen, *J. Am. Chem. Soc.*, 2016, **138**, 3484-3492.
3. C. Zhou, L. Longley, A. Krajnc, G. J. Smales, A. Qiao, I. Erucar, C. M. Doherty, A. W. Thornton, A. J. Hill, C. W. Ashling, O. T. Qazvini, S. J. Lee, P. A. Chater, N. J. Terrill, A. J. Smith, Y. Yue, G. Mali, D. A. Keen, S. G. Telfer and T. D. Bennett, *Nat Commun*, 2018, **9**, 5042.
4. Y. Yang, R. Lin, L. Ge, L. Hou, P. Bernhardt, T. E. Rufford, S. Wang, V. Rudolph, Y. Wang and Z. Zhu, *Dalton Trans*, 2015, **44**, 8190-8197.
5. Y. Yang, L. Ge, V. Rudolph and Z. Zhu, *Dalton Trans.*, 2014, **43**, 7028-7036.
6. R. Lin, L. Ge, H. Diao, V. Rudolph and Z. Zhu, *J. Mater. Chem. A*, 2016, **4**, 6084-6090.
7. R. Lin, L. Ge, H. Diao, V. Rudolph and Z. Zhu, *ACS Appl. Mater. Interfaces*, 2016, **8**, 32041-32049.
8. L. Ge, R. Lin, L. Wang, T. E. Rufford, B. Villacorta, S. Liu, L. X. Liu and Z. Zhu, *Sep. Purif. Technol.*, 2017, **173**, 63-71.
9. M.-T. Vu, R. Lin, H. Diao, Z. Zhu, S. K. Bhatia and S. Smart, *J. Membr. Sci.*, 2019, **587**, 117157.
10. L. Ge, Z. Zhu, F. Li, S. Liu, L. Wang, X. Tang and V. Rudolph, *J. Phys. Chem. C*, 2011, **115**, 6661-6670.